

CCL-TR-95-004

DESY 95-096

May 1995

# Constraints on the Proton's Gluon Distribution from Prompt Photon Production

W. Vogelsang

Rutherford Appleton Laboratory  
Chilton Didcot, Oxon OX11 0QX, England

A. Vogt \*

Deutsches Elektronen-Synchrotron DESY  
Notkestraße 85, D-22603 Hamburg, Germany

## Abstract

We analyze the capability of prompt photon production in  $pp$  and  $p\bar{p}$  collisions to constrain the gluon distribution of the proton, considering data from fixed-target experiments as well as collider measurements. Combined fits are performed to these large- $p_T$  direct- $\gamma$  cross sections and lepton-proton deep-inelastic scattering data in the framework of next-to-leading order perturbative QCD. Special attention is paid to theoretical uncertainties originating from the scale dependence of the results and from the fragmentation contribution to the prompt photon cross section.

\* On leave of absence from Sektion Physik, Universität München, D-80333 Munich, Germany

# 1 Introduction

The production of high- $p_T$  prompt photons in  $pp$  or  $p\bar{p}$  collisions provides an important probe of the proton's gluon distribution,  $g(x, Q^2)$ , due to the presence and dominance of the leading order (LO)  $\mathcal{O}(\alpha\alpha_s)$  'Compton-like' subprocess  $qg \rightarrow \gamma q$ . In fact, constraints on  $g(x, Q^2)$  for  $0.3 \lesssim x \lesssim 0.6$  at  $Q^2 \lesssim 10 \text{ GeV}^2$ , derived mainly from the WA70 fixed-target  $pp \rightarrow \gamma X$  data [1], have been the backbone of the gluon determination in many parton density analyses [2, 3, 4, 5] ever since the pioneering work of [6]. In that paper, a combined next-to-leading order (NLO) fit to the WA70 data and to deep-inelastic scattering (DIS) results from the BCDMS collaboration [7] was performed, and available direct photon data from other fixed-target experiments [8, 9] as well as from ISR [10, 11] and  $Spp\bar{p}S$  [12, 13] were compared to this fit. Since then, major theoretical and experimental developments concerning direct- $\gamma$  production have taken place, and HERA results begin to add DIS constraints in a previously unexplored kinematic region. Therefore, we feel that it is time now for a reanalysis of the prompt photon data and their implications on the gluon density.

Experimentally, much progress has been made during the last years. Some of the direct photon data sets mentioned above have been superseded by improved analyses [14, 15, 16], usually providing smaller statistical and systematic errors. Even more importantly, the accessible range of fractional gluon momenta  $x$  has been considerably enlarged by the recent, partly very precise measurements at the Fermilab Tevatron [17, 18, 19]. By now, the region  $0.01 \lesssim x \lesssim 0.6$  is completely covered, with the data from WA70 [1], R806 [14], UA2 [15] and CDF [18] presently dominating in their respective kinematical regimes. Also, the DIS kinematic coverage has been dramatically improved by the NMC [20] and recent HERA [21, 22]  $F_2^p(x, Q^2)$  structure function data. Quark density measurements, extending down to almost  $x = 10^{-4}$  now, also imply an important constraint on the gluon distribution due to the momentum sum rule. Moreover, scaling violations of  $F_2^p$  at HERA now begin to constrain  $g(x, Q^2)$  severely, especially at  $x \lesssim 0.01$  [23]. Hence it is interesting to examine quantitatively the questions of whether a successful NLO perturbative QCD description of all these data is possible and how much freedom is left for  $g(x, Q^2)$ .

On the theoretical side, it was not yet possible to perform a complete and fully consistent calculation of the NLO prompt photon cross section at the time of the analysis in [6], since the NLO fragmentation contribution, based on the partonic  $2 \rightarrow 3$  QCD subpro-

cesses [24] and on corresponding parton-to-photon fragmentation functions [25, 26], was not yet available. Also, the development of a proper NLO theoretical implementation of isolation cuts [27, 28], imposed on the cross section in the high-energy  $Spp\bar{S}$  and Tevatron experiments, was only recently finished [29] and demonstrated to be phenomenologically important [30]. Even in a very recent global study on direct- $\gamma$  production by members of the CTEQ group [31], the fragmentation pieces are included only in LO and the isolated collider data are transformed to fully inclusive cross sections on this basis.

Finally, the theoretical uncertainties still present in the NLO treatment have not been considered to their full extent in the literature so far. For instance, the dependence of the theoretical cross section on unphysical scales, such as the renormalization scale  $\mu_R$  and the factorization scale  $\mu_F$ , has been treated in the fits of [6, 32] by optimizing the scales using the ‘principle of minimal sensitivity’ [33, 34], i.e., by choosing scales where the NLO cross section is stationary with respect to small changes in  $\mu_R$  and  $\mu_F$ . While this concept certainly is attractive to some extent, see however [27] for a critical discussion, it inevitably does suppress the uncertainty of the theoretical prediction due to the scale dependences. The recent study of [31] has not thoroughly addressed this issue either: in that analysis the scales were included, subject to the constraint  $\mu_R = \mu_F$ , among the parameters fitted to data, which represents just another kind of optimization. There are also other ambiguities, e.g. originating from the experimentally virtually unknown parton-to-photon fragmentation functions. In order to examine the question of how effective the constraints on the gluon distribution coming from prompt photon production really are, it is a crucial issue to take into account such uncertainties inherent to the calculation.

The remainder of this paper is organized as follows: In section 2 we briefly recall the main ingredients needed to calculate the inclusive and isolated prompt photon cross sections in NLO. Section 3 is devoted to a detailed discussion of the main theoretical uncertainties mentioned above and their effects on the calculated cross sections. In section 4 we present combined analyses of an exhaustive set of DIS and prompt photon data in order to arrive at conclusions about the quantitative viability of the NLO framework and about the constraints on the gluon distribution. Finally, we summarize our main findings in section 5.

## 2 General Framework

Two types of processes contribute to the prompt photon production cross section: the so-called ‘direct’ piece, where the photon is emitted via a pointlike (direct) coupling to a quark, and the fragmentation piece, in which the photon originates from the fragmentation of a final state parton. Despite the fact that its corresponding partonic subprocesses are of order  $\alpha_s^2$ , the fragmentation contribution is present already in LO since the parton-to-photon fragmentation functions are effectively of order  $\alpha/\alpha_s$  in perturbative QCD, where  $\alpha$  denotes the fine structure constant. Next order corrections in the strong coupling constant  $\alpha_s$  have been calculated in the  $\overline{\text{MS}}$  renormalization and factorization schemes for both the direct [28, 33, 35] and the fragmentation [24] subprocesses, hence the cross sections can be consistently calculated to order  $\alpha\alpha_s^2$ . The cross section for the fully inclusive production of a prompt photon with momentum  $p_\gamma$  schematically reads

$$d\sigma \equiv d\sigma_{dir} + d\sigma_{frag} = \sum_{a,b=q,\bar{q},g} \int dx_a dx_b f_a(x_a, \mu_F^2) f_b(x_b, \mu_F^2) \times \quad (1)$$

$$\left[ d\hat{\sigma}_{ab}^\gamma(p_\gamma, x_a, x_b, \mu_R, \mu_F, M_F) + \sum_{c=q,\bar{q},g} \int_{z_{min}}^1 \frac{dz}{z^2} d\hat{\sigma}_{ab}^c(p_\gamma, x_a, x_b, z, \mu_R, \mu_F, M_F) D_c^\gamma(z, M_F^2) \right]$$

where  $z_{min} = x_T \cosh \eta$  with the prompt photon’s rapidity  $\eta$ , and  $x_T = 2p_T/\sqrt{s}$ . In eq. (1),  $d\hat{\sigma}_{ab}^i$  represent the subprocess cross sections for partons  $a, b$  producing a particle  $i$  ( $i = \gamma, q, g$ ), integrated over the full phase space of all other final state particles.  $f_i(x, \mu_F^2)$  denotes the number density of the parton type  $i$  in the proton (or antiproton) at momentum fraction  $x$  and scale  $\mu_F$ , and  $D_c^\gamma(z, M_F^2)$  is the photon fragmentation function at scale  $M_F$ ,  $z$  being the fraction of energy of the fragmenting parton  $c$  transferred to the photon.

As already mentioned in the introduction and made explicit in eq. (1), the cross section in any fixed order of perturbation theory depends on unphysical scales which have to be introduced in the procedure of renormalization ( $\mu_R$ ) and of factorization of initial ( $\mu_F$ ) and final ( $M_F$ ) state mass singularities. The latter type of singularities appears, e.g., in the calculation of the  $\mathcal{O}(\alpha_s^3)$   $ab \rightarrow cde$  NLO fragmentation subprocess cross sections when the parton  $c$  (which then fragments into the photon) becomes collinear with particle  $d$  or  $e$ , but also in the calculation of the  $\mathcal{O}(\alpha\alpha_s^2)$   $ab \rightarrow \gamma de$  NLO ‘direct’ subprocess cross sections when the photon and a final state quark are collinear. These singularities need to be factorized at a scale  $M_F$  into the ‘bare’ fragmentation functions in order to render the cross section finite. The fragmentation functions then obey corresponding

NLO evolution equations. Since factorizing singularities is not a unique procedure but depends on the factorization prescription adopted, it becomes obvious that only the sum of the direct and the fragmentation pieces is a physical (scheme independent) quantity beyond the LO, but not these parts individually. In particular, even if the fragmentation contribution turns out to be numerically small, its addition on a LO basis to a NLO ‘direct’ piece is theoretically inconsistent and yields a scheme dependent cross section. Needless to say that a consistent NLO calculation also affords parton distributions and photon fragmentation functions evolved according to their respective NLO evolution equations. For calculating these  $Q^2$ -evolutions we use the Mellin- $n$  space technique described in [36].

At very high-energy  $p\bar{p}$  colliders the photon is experimentally required to be ‘isolated’ in order to suppress the huge background due to copious production of  $\pi^0$ , the decay of which can fake a prompt photon event. This means that the amount of hadronic energy  $E_{had}$  allowed in a cone  $\sqrt{(\Delta\phi)^2 + (\Delta\eta)^2} \leq R$  around the photon direction is limited to a small fraction of the photon energy,  $E_{had} \leq \epsilon E_\gamma$  with  $\epsilon \lesssim 0.1$ . In order to compare QCD predictions with isolated collider data, the theoretical calculation has to include this isolation criterion which leads to a significant decrease from the fully inclusive cross section [29, 37]. In [29] a simple, yet accurate way of incorporating the isolation cut into the NLO calculation has been developed. Starting from the fully inclusive cross section, the isolated one is obtained by introducing a subtraction term [27, 29],

$$d\sigma^{isol}(R, \epsilon) = d\sigma^{incl} - d\sigma^{sub}(R, \epsilon) \quad , \quad (2)$$

where  $d\sigma^{sub}(R, \epsilon)$  is the cross section for having *more* hadronic energy than  $\epsilon E_\gamma$  in the cone around the photon. It turns out that  $d\sigma^{sub}(R, \epsilon)$  can be easily and reliably calculated in the approximation of a rather narrow cone. An equation similar to eq. (2) (which holds for the NLO direct contributions) can also be written down for the NLO fragmentation piece [29], in which case the main effect of imposing the isolation cut is to raise the lower integration limit in eq. (1) to  $z_{min} = 1/(1 + \epsilon)$ . In this way, it is possible to calculate also the isolated prompt photon production cross section measured at high-energy colliders in a consistent way beyond the leading order.

We conclude this section by noting that the recent study in [31] reports a (rather  $p_T$  independent)  $\mathcal{O}(10\%)$  discrepancy between the NLO programs of [28] and [35] in the kinematic regime of the CDF measurements, which persists also if the fully inclusive cross section is considered [38]. In this context it is interesting to mention that there is no such discrepancy between the two calculations of [33] and [35], which are in *exact* agreement

concerning the NLO direct contribution to the fully inclusive cross section for all  $p_T$  and  $\sqrt{s}$ . For all calculations to follow we use the program of [35] for the direct part of the NLO prompt photon cross section, along with the expressions of [24] for the fragmentation contribution. When calculating the isolated cross section we complement these programs according to the prescription of [29].

### 3 Theoretical Uncertainties

In this section, we address the main uncertainties entering the NLO calculation of the prompt photon cross section, namely the dependence on the photon fragmentation functions and on the renormalization and mass factorization scales. As a point of reference, we first calculate the cross section for a fixed ‘standard’ set of input distributions and parameters and confront it with the data. For this purpose, the parton distributions and photon fragmentation functions are taken from GRV [4, 26], together with the value of the QCD scale parameter for four active flavours,  $\Lambda_{\overline{\text{MS}}}^{(4)} = 200$  MeV. We choose  $\mu_R = \mu_F = M_F = p_T/2$  for the renormalization and factorization scales except for the isolated prompt photon data, where  $M_F = Rp_T$  seems more appropriate [27].

The very small charm effects in the cross section at fixed-target and ISR energies are neglected. For the  $Spp\bar{p}S$  and the Tevatron experiments, however, charm-induced contributions coming, e.g., from  $cg \rightarrow \gamma c$  are not negligible. We employ the effective (massless) charm quark distribution of [3] in calculating these contributions. We have checked that reasonable variations of this charm density do not significantly alter our results. An alternative approach to the heavy quark (charm) contribution is to perform mass factorization only for the light  $u$ ,  $d$ , and  $s$  quarks. In this scheme, also used in [4], the heavy flavours  $c$ ,  $b$ ,  $\dots$  do not act as partons in the proton, and in LO charmed prompt photon events are only introduced via the processes  $gg \rightarrow \gamma c\bar{c}$  and  $q\bar{q} \rightarrow \gamma c\bar{c}$  with *massive* charm quarks. The results of [39] show, however, that these two approaches yield very similar results at least in LO. Thus the theoretical uncertainty originating from the charm treatment seems to be rather small. For the rest of this paper, we therefore use the fixed intrinsic charm quark distribution of [3] which facilitates the calculations.

The sets of experimental data we take into account in this section are the fixed-target data of WA70 [1] ( $\sqrt{s} = 24$  GeV,  $pp$  inclusive), the ISR results from R806/7 [14] ( $\sqrt{s} = 63$

GeV,  $pp$  inclusive), the  $Spp\bar{p}S$  results from UA2 [15] ( $\sqrt{s} = 630$  GeV,  $p\bar{p}$  isolated) and the Tevatron data of CDF [18] ( $\sqrt{s} = 1.8$  TeV,  $p\bar{p}$  isolated with  $R = 0.7$  and  $\epsilon = 2$  GeV/ $p_T$ ). As mentioned above, these data sets dominate in their respective kinematical domains. The cross sections of [1] and [18] have been averaged over the experimentally covered regions of rapidity  $\eta$ , while the results in [14] and [15] have been presented at  $\eta = 0$ . For our comparisons and fits, we add the statistical and systematic errors in quadrature, using point-to-point errors where these are separately available [15, 18]<sup>1</sup>. Fig. 1 displays the results for our ‘standard’ choice of input distributions and parameters. We show the ‘default quantity’ (data – theory)/theory versus  $x_T$ . This provides a particularly easy visualization of the (dis)agreement between data and theoretical calculation in view of the strong  $p_T$  fall-off of the cross section.  $x_T$  is a good representative of the Björken- $x$  values predominantly probed in the gluon distribution at given  $p_T$  and  $\sqrt{s}$ .

As can be seen from Fig. 1, the overall agreement between data and the NLO theoretical prediction is good though not complete, especially if the very small errors of the CDF data are taken at face value. The agreement between theory and the fixed-target and ISR measurements is very good, whereas the comparison with the high-energy collider results seems to be slightly less successful, since both the CDF and the UA2 data show a somewhat stronger rise for small  $x_T$  than the theoretical cross section<sup>2</sup>. This effect is more pronounced and statistically more meaningful for the CDF results, which possess the smallest point-to-point errors of all data sets and therefore provide a very precise measurement of the *slope* of the cross section. Note that the CDF [18] as well as the UA2 [15] data are subject to a normalization uncertainty of about 10% which we have used in the figure to center the results on the zero line. It has to be emphasized that a *much* stronger discrepancy between high-energy collider data and NLO calculations was reported previously [17, 18]. As was shown in [30], a dramatic improvement is obtained by using ‘modern’ sets of (steep) parton distribution functions like, e.g., those of GRV [3, 4] or the most recent MRS(A',G) sets [2] as well as, equally important, by including a properly isolated *NLO* fragmentation contribution in the calculation. According to Fig. 1, the latter amounts to a 20% slope effect for CDF conditions, thus its inclusion is clearly crucial for a quantitative comparison between the experimental and theoretical cross sections. The fragmentation piece is non-negligible *despite* the presence of the iso-

<sup>1</sup>We thank S. Kuhlman for providing the break-up of the systematic errors of the CDF direct photon data into a point-to-point and a fully correlated part.

<sup>2</sup>Note, however, that there is good agreement between NLO theory and the preliminary Tevatron D0 results [19], which on the other hand have sizeably larger errors than the CDF data [18].

lation cut without which it would easily contribute about 50% to the total cross section [25, 30, 37]. The results in Fig. 1 indicate a (minor) remaining discrepancy between the  $p_T$ -slopes of the experimental and theoretical cross sections even after the improvements of [30] have been applied. One furthermore infers from the figure that fragmentation also plays an important role in the calculations in the ISR and fixed-target regions, where no isolation cut has been applied. Here it leads to an effect of partly even more than 20%, but influences the slope to a lesser extent.

An important uncertainty in the calculation is the dependence of the cross section on the parton-to-photon fragmentation functions which are experimentally unknown so far. Two partly very different NLO sets of such distributions have been suggested in the literature, namely in [25] (ACFGP) and in [26] (GRV). Fig. 2 presents  $D_u^\gamma$  and  $D_g^\gamma$  from both groups at two scales relevant for our comparisons to data. In both [25] and [26], the fragmentation functions are assumed to evolve from a pure vector meson dominance (VMD) input at some very low scale. However, this boundary condition for  $D_i^\gamma(z, Q^2)$  has been implemented in rather different factorization schemes. ACFGP use the  $\overline{\text{MS}}$  scheme, whereas GRV impose the VMD input in the timelike version of the so-called  $\text{DIS}_\gamma$  scheme, originally introduced for the (spacelike) parton structure of the photon [40]. In the  $\overline{\text{MS}}$  scheme employed here the latter ansatz corresponds to an additional, rather large input for  $D_q^\gamma$ , which guarantees the positivity of the timelike structure function  $f_1^{(T)}$  for single photon inclusive  $e^+e^-$  annihilation,  $e^+e^- \rightarrow \gamma X$ . Thus the quark-to-photon fragmentation functions of GRV [26] are larger than the ones of ACFGP [25], especially at low scales, despite the fact that in [25] a sizeably larger VMD input is employed. On the other hand,  $D_g^\gamma$  of ACFGP is much larger than its GRV counterpart. This is due to the *huge* VMD gluonic input in [25], based on the assumption  $D_g^{\rho^0} = D_g^{\pi^0}$  with  $\int_0^1 dz z D_g^{\pi^0}(z, 2 \text{ GeV}^2) = 0.5$ , meaning that as much as half of an outgoing gluon's momentum is carried away by neutral pions alone.

The effects of these differences are displayed in Fig. 3, where we show the (scale and scheme dependent) relative importance of the fragmentation part of the prompt photon cross sections for ISR and Tevatron energies both for the total and for the gluon initiated contributions. We have normalized all results to the direct cross section, and apart from the fragmentation functions, all parameters and distributions have been chosen as in the ‘standard’ calculation above. As already obvious from Fig. 1, the ACFGP [25] and GRV [26] fragmentation functions yield very similar results for the total fragmentation contribution. For the isolated Tevatron case,  $g \rightarrow \gamma$  fragmentation plays an almost



negligible role due to the high  $z_{min}$  cut implied by the isolation criterion, e.g.  $z_{min} = (1 + 2 \text{ GeV}/p_T)^{-1}$  for CDF conditions. The  $q \rightarrow \gamma$  pieces are rather similar, since  $D_q^\gamma(z, Q^2)$  is probed at large  $z$  and  $Q^2$  here. In the fully inclusive ISR case, on the other hand,  $z_{min} = x_T = 2p_T/\sqrt{s} \gtrsim 0.15$  for  $\eta = 0$ , and the huge difference in  $D_g^\gamma$  between [25] and [26] enters the fragmentation cross section. However, since the scales  $Q^2 \approx p_T^2/4$  are rather low here, this effect is strongly compensated by the difference in the quark contributions. Of course, the difference in the total results is not necessarily fully representative of the uncertainty originating in the fragmentation part of the cross section. We have checked that in the theoretically more realistic GRV [26] case, a 50% change in the VMD input distributions for  $D_i^\gamma$  has no sizeable effect on the results due to the dominance of  $D_q^\gamma$ . Hence we will keep the fragmentation functions of [26] for the rest of this paper. Clearly, experimental information on the fragmentation functions, e.g. from  $e^+e^- \rightarrow \gamma X$  [41], is needed.

Let us now discuss the scale dependence of the results, i.e. the changes in the theoretical predictions for varying  $\mu_R$  and  $\mu_F$ . It turns out that the NLO cross section depends only *very* weakly on  $M_F$  both for the isolated [29] and the fully inclusive cases. For the latter, e.g., the difference of the results for  $M_F = p_T/2$  and  $M_F = p_T$  at fixed  $\mu_R, \mu_F$  does not exceed 1%. We therefore keep the fragmentation scale  $M_F$  fixed at  $M_F = p_T/2$  for the fixed-target and ISR experiments and  $M_F = Rp_T$  for the isolated cross sections in the following. The dashed and the dash-dotted lines in Fig. 4 display the shifts in the theoretical results if we choose  $\mu_R = \mu_F = 0.3 p_T$  or  $\mu_R = \mu_F = 1.0 p_T$ , respectively, instead of  $\mu_R = \mu_F = p_T/2$ . More precisely, the curves show  $(\sigma'_{th} - \sigma_{th})/\sigma_{th}$ , where  $\sigma'_{th}$  is the theoretical cross section as calculated with the new values for the scales, whereas  $\sigma_{th}$  corresponds to the ‘standard’ calculation. It becomes obvious that the results for  $\mu_R = \mu_F = 0.3 p_T$  or  $1.0 p_T$  amount to almost a constant shift in the normalization of the theoretical cross section as far as the CDF and UA2 data are concerned, and do not provide a change in the slope of the cross section. It can also be seen that the theoretical cross section at lower energies shows a rather strong scale dependence. So far, our results are in agreement with the claims in [18, 31] that scale uncertainties provide (almost) no effect on the  $p_T$ -shape in the collider case.

There is, however, no argument that enforces  $\mu_R$  and  $\mu_F$  to be exactly equal, they are just expected to be of the same order of magnitude, given by the prompt photon’s  $p_T$ . In fact,  $\mu_R \neq \mu_F$  automatically happens if one uses ‘optimized’ scales [33] as mentioned in the introduction. A smaller renormalization scale  $\mu_R$  along with a larger factorization

scale  $\mu_F$  can be expected to create a steeper slope of the theoretical result, since lowering  $\mu_R$  mainly increases the strong coupling constant  $\alpha_s$ , whereas the main effect of a larger  $\mu_F$  is to deplete the gluon distribution at larger  $x$  and to increase it at smaller  $x$ . In fact, the curves in Fig. 4 show that these effects are quite significant. The choices of, e.g.,  $\mu_R = 0.3 p_T$ ,  $\mu_F = p_T$  or  $\mu_R = p_T$ ,  $\mu_F = 0.3 p_T$  do lead to about  $\pm 20\%$  shape changes in the CDF region, respectively. Obviously, scale dependences *are* able to affect the  $p_T$ -slope of the NLO cross section, contradicting the corresponding conclusions drawn in [18, 31] which were derived assuming  $\mu_R = \mu_F$ . All in all, scale changes seem to have a rather strong influence on the theoretical cross section even beyond the LO. This is in line with the observations in [27], where it was shown that at small  $x_T$  the scale dependence is only slightly reduced when going from LO to NLO, which renders it difficult to estimate the most appropriate scales. The scale dependence of the NLO cross section for prompt photon production indicates the importance of corrections of even higher order and sets severe limits on the accuracy of gluon determinations from these data.

## 4 Combined Analysis of DIS and Prompt Photon Data

In this section, we examine the question of whether the agreement between NLO calculation and the isolated prompt photon data can be further improved by adapting the proton's parton content, in particular its gluon density. For this purpose, we perform combined NLO fits to direct- $\gamma$  production and DIS structure function data, the latter pinning down the quark densities, with different choices for the renormalization and factorization scales. In this way, we also investigate the uncertainty of the resulting gluon distribution originating from the scale dependence of the prompt photon cross section.

Technically we proceed as follows: at the reference scale of  $Q_0^2 = 4 \text{ GeV}^2$  the gluon input is parametrized as

$$xg(x, Q_0^2) = A_g x^{\alpha_g} (1-x)^{\beta_g} (1 + \gamma_g \sqrt{x} + \delta_g x) \quad . \quad (3)$$

This functional form is also used in the latest MRS analysis [2]. For each given set of  $\alpha_g$ ,  $\beta_g$ ,  $\gamma_g$ , and  $\delta_g$ , a fit of the quark densities to  $F_2^p$  data is performed, where  $A_g$  is fixed by the energy-momentum sum rule. Here the non-singlet quark densities  $u_v = u - \bar{u}$ ,  $d_v = d - \bar{d}$  and  $\Delta = \bar{d} - \bar{u}$  are, as in [4], for  $\Lambda_{\overline{\text{MS}}}^{(4)} = 200 \text{ MeV}$  directly adopted from the

MRS(A) global fit [2]. For other values of  $\Lambda$  we employ the modified non-singlet sets of [42]. This procedure guarantees a sufficiently accurate description of all observables testing mainly the flavor decomposition of the quark content and facilitates the fitting procedure since it reduces the number of free parameters. The sea quark input is parametrized as [2]

$$\begin{aligned} x(\bar{u} + \bar{d})(x, Q_0^2) &= A_\xi x^{\alpha_\xi} (1-x)^{\beta_\xi} \left(1 + \gamma_\xi \sqrt{x} + \delta_\xi x\right) \ , \\ xs(x, Q_0^2) &= \frac{1}{4} x(\bar{u} + \bar{d})(x, Q_0^2) \ . \end{aligned} \quad (4)$$

This input is evolved in the factorization scheme of [4] (see section 3), calculating the charm contribution to  $F_2$  via the LO Bethe-Heitler process using the LO gluon distribution and  $\Lambda_{LO}$  of [4]. The five parameters in eq. (4) are fitted to the available  $F_2^p$  data of BCDMS [7, 43], NMC [20], ZEUS [21], and H1 [22] in the region where the structure function is sensitive to the sea quark and gluon densities,  $x \leq 0.3$ , and where higher twist contributions are expected to be small,  $Q^2 \geq 5 \text{ GeV}^2$ . As in [2] the BCDMS data are normalized down by 2%. At the present level of experimental accuracy, the HERA  $F_2^p$  normalization uncertainties [21, 22] can be disregarded for our purpose. Statistical and systematic errors are added quadratically for all data sets.

We then use the complete set of parton distributions obtained from this  $F_2^p$  fit for a fixed gluon shape to determine the  $\chi_{dir.\gamma}^2$  for the prompt photon data of WA70, R806/7, UA2 and CDF [1, 14, 15, 18], already discussed in section 3, supplemented by the  $pp$  inclusive results of NA24 [8] and UA6 [16], both at  $\sqrt{s} = 24 \text{ GeV}$ . Due to the very small point-to-point errors of the CDF data [18] their overall normalization uncertainty is rather important. Therefore it is allowed to float in the fit with a contribution to  $\chi_{dir.\gamma}^2$  according to its experimental uncertainty of 10%, see [5]. All other data sets, including [8, 15] where separate normalization uncertainties are provided, are fixed at their nominal normalization. The whole procedure is repeated until finally  $\chi_{tot}^2 = \chi_{DIS}^2 + \chi_{dir.\gamma}^2$  is minimized. We have chosen this two-step approach of two ‘nested’ fits since it affords the least number of evaluations of  $\chi_{dir.\gamma}^2$  which dominate the consumed computer time due to the complexity of the NLO prompt photon cross section calculation. In order to examine the uncertainty coming from the choice of the QCD scale parameter  $\Lambda$ , we perform fits for  $\Lambda_{\overline{\text{MS}}}^{(4)} = 200 \text{ MeV}$  and  $300 \text{ MeV}$ . These values are representative of the present range of  $\Lambda$  found in analyses of DIS and related data [2, 43, 44, 45]. In view of our findings for the scale dependence of the prompt photon cross section obtained in the last section, we repeat the fits for various combinations of the renormalization/factorization scales,

systematically scanning the range  $0.3 p_T \leq \mu_R, \mu_F \leq 2.0 p_T$ , see below for a detailed discussion.

Fig. 5 displays the results of three of our fits, again compared to the data of [1, 14, 15, 18]. For clarity, the additional large- $x_T$  data sets of [8, 16] are not shown in the figure. The upper part presents the fit using the ‘standard’ scales and  $\Lambda_{\overline{\text{MS}}}^{(4)}$  of section 3, the lower plot depicts further examples of best possible fits, one for each  $\Lambda$ -value employed. The latter two fits happen to lead to the same CDF normalization factor of +10%. The input parameters and  $\chi^2$ -results for these three representative fits are given in Table 1. It is obvious that we obtain good fits, with  $\chi^2$  per data point slightly below 1 also in the prompt photon subset of the fitted data. The ISR and fixed-target data [1, 8, 14, 16] are described about as well as in the reference calculation in section 3. The  $\chi^2$  for the CDF results [18] seems to remain a bit high. We have not been able to reach a value below 25 for the 16 data points, however with more than 10 units contributed by just the measurement at  $p_T = 48.9$  GeV. The figure clearly demonstrates that *no* shape problem remains here. With respect to the UA2 results [15], the situation does only slightly improve; with present errors, however, the UA2 data do not impose strong constraints on the fits. On the other hand, it should be noted that a data set with about the same central values but much smaller errors would, in combination with the CDF results, very seriously challenge the NLO framework used in this paper, since we have been unable to improve the description sizeably even by artificially reducing the UA2 errors in special runs of our fits. For the larger value of  $\Lambda_{\overline{\text{MS}}}^{(4)}$ , the range of renormalization and factorization scales giving very good fits to the data is somewhat shifted towards larger values. As can be seen from Fig. 5 and the table, we do not find a significant difference in the quality of the fits for the two  $\Lambda$ -values. Taking into account the full scale dependence of the NLO cross section reduces the sensitivity of the prompt photon data to  $\alpha_S$  as compared to, e.g., [6, 32] where ‘optimized’ scales were used.

Our results demonstrate that presently published data on  $pp, p\bar{p} \rightarrow \gamma X$  can be described quantitatively by NLO perturbative QCD. This finding is at variance with the results of a recent, partly comparable analysis of the CTEQ group [31]. In that paper, it is concluded that (at least) the  $p_T$ -shapes of the ISR and collider data cannot be satisfactorily fitted, unless an ‘intrinsic’  $k_T$ -smearing is introduced, which is as large as  $\langle k_T \rangle \approx 4$  GeV for  $Spp\bar{S}$  and Tevatron conditions. It should be clear that we do not claim positive evidence for the absence of such a (somewhat counterintuitive) smearing, we just state that the data considered here can be accounted for without this assumption. It should

$\Lambda^{(4)}/\text{MeV}$	200	200	300
$\mu_R/p_T$	0.5	0.3	0.7
$\mu_F/p_T$	0.5	0.7	0.7
$\alpha_g$	-0.011	-0.125	-0.080
$\beta_g$	5.715	5.314	5.024
$\gamma_g$	-4.174	-4.200	-3.963
$\delta_g$	5.217	5.370	4.931
$A_\xi$	0.768	0.775	0.787
$\alpha_\xi$	-0.156	-0.148	-0.135
$\beta_\xi$	7.480	7.641	7.173
$\gamma_\xi$	0.642	0.740	0.843
$\delta_\xi$	1.521	1.622	1.080
$\chi_{DIS}^2$	253.6	257.3	254.4
$\chi_{dir.\gamma}^2$	59.1	52.8	56.5
$\chi_{tot}^2$	312.7	310.1	310.9

Table 1: Input parameters for eqs. (3) and (4) for three representative combined fits to direct- $\gamma$  and  $F_2^p$  data, together with the resulting  $\chi^2$ -values for the 60 prompt photon and 294 DIS data points.

be noted in this context, however, that a  $\langle k_T \rangle$  of about 1 GeV for fixed-target energies would spoil [46] the successful description of the WA70 data [1]. The consequences of our optimal ‘pure’ NLO fits to all direct photon data will be elucidated below.

Let us note before some obvious differences between our study and [31]. With respect to data, we use the latest results of R806/7 [14], whereas [31] includes previous superseded steeper results of this collaboration [11]. Taking into account the results of [14], there is obviously no slope offset between NLO theory and ISR data, neither for ‘standard’ distributions, see Fig. 1 and the last reference of [2], nor for our fits discussed above. In the fixed-target region, we do not include the recent E706 data [47] from  $pBe$  collisions in order to avoid any bias from a possible EMC-like effect on the nuclear gluon density. With respect to the theoretical treatment, in contrast to [31] we fully incorporate *NLO* fragmentation and the corresponding treatment of isolation into our analysis. The very small errors of the CDF data [18] make a complete and consistent NLO analysis mandatory in order to arrive at any solid statements on the viability of the NLO description of prompt

photon production.<sup>3</sup>

Hence in the present situation it seems reasonable to us to maintain the ‘pure’ NLO perturbative QCD framework and to investigate the consequences of optimal fits to the direct- $\gamma$  data in this scenario. In Fig. 6 the gluon distributions obtained in the three fits displayed above are compared at  $Q^2 = 20 \text{ GeV}^2$  to the corresponding result of the recent MRS(A’) global study [2] where only fixed-target prompt- $\gamma$  data were included in the analysis. Although data at different  $p_T$  probe the parton distributions at different scales, the main effect of including the CDF results [18] is readily seen in the figure. The gluon distribution is increased at the lower end of the  $x$ -range accessed by these measurements,  $x \simeq 0.01$ , and is decreased around  $x \simeq 0.15$ , thereby in between providing the steeper rise suggested by the data. At very small  $x$ ,  $x \lesssim 10^{-3}$ , our gluon densities are larger than the one of MRS(A’) and more similar in magnitude to the MRS(G) [2] and GRV [4] parametrizations.

Effects of such an enhanced gluon density at  $x \approx 10^{-2}$  should also show up in other processes which are sensitive to  $g(x, Q^2)$  in that  $x$ -region such as, e.g, bottom production in high-energy  $p\bar{p}$  collisions at the Tevatron. Fig. 7 illustrates this fact. The cross section for single-inclusive  $b$ -quark production,  $\sigma(p\bar{p} \rightarrow bX)$ , expected to be mainly driven by gluon-gluon fusion, has been measured as a function of the minimal transverse momentum  $p_T^{min}$  of the  $b$ -quark by the CDF and D0 collaborations recently [48, 49]. The figure shows these data together with corresponding NLO calculations based on the work of [50, 51] for two of our fitted parton distribution sets and the MRS(A’) parametrization [2]<sup>4</sup>. For this illustration, we have chosen  $\mu = \frac{1}{2}\sqrt{p_T^2 + m_b^2}$  for the renormalization and factorization scales and  $m_b = 4.5 \text{ GeV}$  for the bottom mass. Note that the theoretical uncertainties from variations of these parameters are rather substantial [48, 49].

Let us finally come back to the scale dependence of the fitted gluon densities. As already mentioned above, we have scanned the scale range  $0.3 p_T \leq \mu_R, \mu_F \leq 2.0 p_T$  in our fits. The lower limit has been introduced in order to avoid low scales below about 1 GeV. We find very good combined fits to the complete set of prompt photon production and DIS structure function data given above for  $0.3 (0.5) \lesssim \mu_R, \mu_F/p_T \lesssim 0.7 (1.0)$  for  $\Lambda^{(4)} = 200 \text{ MeV}$  (300 MeV), respectively, and  $\mu_R \lesssim \mu_F$ . The spread of the gluon distributions of all

---

<sup>3</sup>The input form used in the fits of [31] has not been given in the paper. In the likely case that the CTEQ3 [5] input ansatz has also been employed in [31], another difference with respect to our study would be added, since we find that the inclusion of the  $\sqrt{x}$ -term in (3), not present in [5], is important.

<sup>4</sup>We thank M. Stratmann for performing these calculations.

these best fits can serve as a measure for the theoretical uncertainty on  $xg(x, Q^2)$  induced by scale variations. Fig. 8 displays the resulting ‘error band’, normalized to the MRS(A’) gluon distribution [2] at  $Q^2 = 20 \text{ GeV}^2$ . Also shown are the uncertainties at four selected  $x$ -values arising from the experimental errors. They have been determined from fits for one scale combination, which are one unit in the total  $\chi^2$  higher than the corresponding best fit. In view of the controversial theoretical interpretation [30, 31] of the isolated high-energy collider data [15, 18], we have repeated the fits for the theoretical error band retaining only the 30 (non-isolated) fixed-target and ISR data points of [1, 8, 11, 16] in the direct- $\gamma$  part of the analyses. The resulting band is also presented in Fig. 8.

It becomes obvious from the figure that the same pattern of deviations from the MRS(A’) fit [2], namely an increase (decrease) at  $x$  around 0.01 (0.15), is present for all scale choices which allow for a good fit of the complete set of prompt photon data. Thus this effect is significant and cannot be removed by a ‘better’ choice of scales. Not too surprisingly, the fits restricted to the non-isolated data lead to gluon densities considerably closer to standard distributions. They are, taking into account the experimental uncertainties, in fact in good agreement with, e.g., the GRV gluon parametrization [4] employed as a standard choice in section 3. At  $x < 0.1$ , the experimental uncertainties and the theoretical error bands of the fits to all data are of about the same size. However, in the classical fixed-target regime,  $x > 0.3$ , mainly considered in [6] and many subsequent analyses via ‘optimized’ scales [33], the uncertainty of  $g(x, Q^2)$  is dominated by scale variations. For instance, at  $x \simeq 0.4$ , the spread of the fitted gluon densities is as large as almost a factor of two. In this large- $x$  region, shown separately in Fig. 9 also for a high scale typical for the production of particles with masses of a few hundred GeV, a comparison of recent parametrizations, e.g. of MRS(A’,G) and GRV [4] as displayed in Fig. 8, does not indicate the real uncertainty of the gluon distribution.

## 5 Conclusions

We have performed a detailed NLO perturbative QCD study of prompt photon production in  $pp$  and  $p\bar{p}$  collisions with respect to its sensitivity to the proton’s gluon content. In fact, our analysis is the first one that includes both the full NLO treatment of the fragmentation contribution and the complete NLO treatment of isolation, and the consideration of the full information available now from experiment. We have carefully studied the theoretical

uncertainties, especially those arising from the so far experimentally unknown parton-to-photon fragmentation functions and from scale variations.

The dependence of the theoretical cross sections on the renormalization and factorization scales turns out to be the dominant source of uncertainty. Particularly at large- $x$ ,  $x > 0.3$ , the scale dependence very severely limits the accuracy of NLO gluon determinations from (fixed-target) prompt- $\gamma$  production data. Present-day gluon parametrizations of CTEQ3, GRV, and MRS(A',G) are very similar in this region and their difference does not represent the real uncertainty of  $g(x, Q^2)$  here. The isolated direct- $\gamma$  cross sections are also sizeably affected by the choice of these scales in magnitude and  $p_T$ -shape.

We have carried out combined global analyses of fixed-target and collider prompt-photon cross sections and DIS structure function data within the perturbative NLO framework. We find that such combined fits work very well and give a good description of all prompt photon data for various combinations of renormalization and factorization scales and values of the QCD scale parameter  $\Lambda$ . The gluon distributions resulting from such fits turn out to be larger at  $x \approx 0.01$  and smaller at  $x$  around 0.15 than those obtained in recent global analyses of parton distributions not taking into account the full set of prompt photon data.

## Acknowledgements

We thank M. Glück and E. Reya for useful discussions. This work was supported in part by the German Federal Ministry for Research and Technology under contract No. 05 6MU93P.



## References

- [1] M. Bonesini et al., WA70 Collab., Z. Phys. **C38** (1988) 371.
- [2] A.D. Martin, W.J. Stirling and R.G. Roberts, Phys. Rev. **D47** (1993) 867; Phys. Lett. **B306** (1993) 145; Phys. Rev. **D50** (1994) 6734 [MRS(A)]; Rutherford Appleton Lab report RAL-95-021 [MRS(A',G)].
- [3] M. Glück, E. Reya and A. Vogt, Z. Phys. **C53** (1992) 127.
- [4] M. Glück, E. Reya and A. Vogt, DESY 94-206 and Univ. Dortmund report DO-TH 94/24, to appear in Z. Phys. **C**.
- [5] J. Botts et al., CTEQ Collab., Phys. Lett. **B304** (1993) 159; H.L. Lai et al., CTEQ Collab., Phys. Rev. **D51** (1995) 4763.
- [6] P. Aurenche, R. Baier, M. Fontannaz, J.F. Owens and M. Werlen, Phys. Rev. **D39** (1989) 3275.
- [7] A.C. Benvenuti et al., BCDMS Collab., Phys. Lett. **B223** (1989) 485.
- [8] C. De Marzo et al., NA24 Collab., Phys. Rev. **D36** (1987) 8.
- [9] A. Bernasconi et al., UA6 Collab., Phys. Lett. **B206** (1988) 163.
- [10] A.L.S. Angelis et al., R108 Collab., Phys. Lett. **94B** (1980) 106; A.L.S. Angelis et al., R110 Collab., Nucl. Phys. **B327** (1989) 541.
- [11] E. Anassontzis et al., R806 Collab., Z. Phys. **C13** (1982) 277.
- [12] C. Albajar et al., UA1 Collab., Phys. Lett. **B209** (1988) 385.
- [13] R. Ansari et al., UA2 Collab., Z. Phys. **C41** (1988) 395.
- [14] T. Akesson et al., R806 Collab., Sov. J. Nucl. Phys. **51** (1990) 836.
- [15] J. Alitti et al., UA2 Collab., Phys. Lett. **263B** (1991) 544.
- [16] G. Balocchi et al., UA6 Collab., Phys. Lett. **317B** (1993) 243,250.
- [17] F. Abe et al., CDF Collab., Phys. Rev. Lett. **68** (1992) 2734.
- [18] F. Abe et al., CDF Collab., Phys. Rev. Lett. **73** (1994) 2662.

- [19] J. Kotcher, D0 Collab., talk presented at the *9th Workshop on Proton-Antiproton Collider Physics*, Tsukuba, Japan, 1993, FERMILAB-Conf-93/387-E.
- [20] P. Amaudruz et al., NMC Collab., Phys. Lett. **B295** (1992) 159.
- [21] M. Derrick et al., ZEUS Collab., Phys. Lett. **B316** (1993) 412; Z. Phys. **C65** (1995) 379.
- [22] I. Abt et al., H1 Collab., Nucl. Phys. **B407** (1993) 515; T. Ahmed et al., H1 Collab., DESY 95-006.
- [23] M. Derrick et al., ZEUS Collab., Phys. Lett. **B345** (1995) 576.
- [24] F. Aversa, P. Chiappetta, M. Greco and J.Ph. Guillet, Phys. Lett. **B210** (1988) 225; Phys. Lett. **B211** (1988) 465; Nucl. Phys. **B327** (1989) 105.
- [25] P. Aurenche, P. Chiappetta, M. Fontannaz, J.Ph. Guillet and E. Pilon, Nucl. Phys. **B399** (1993) 34.
- [26] M. Glück, E. Reya and A. Vogt, Phys. Rev. **D48** (1993) 116.
- [27] E.L. Berger and J. Qiu, Phys. Lett. **B248** (1990) 371; Phys. Rev. **D44** (1991) 2002.
- [28] H. Baer, J. Ohnemus and J.F. Owens, Phys. Lett. **B234** (1990) 127; Phys. Rev. **D42** (1990) 61.
- [29] L.E. Gordon and W. Vogelsang, Phys. Rev. **D50** (1994) 1901.
- [30] M. Glück, L.E. Gordon, E. Reya and W. Vogelsang, Phys. Rev. Lett. **73** (1994) 388.
- [31] J. Huston et al., Michigan State Univ. report MSU-HEP-41027 and CTEQ-407 (1995).
- [32] A.D. Martin, W.J. Stirling and R.G. Roberts, Phys. Rev. **D43** (1991) 3648.
- [33] P. Aurenche, R. Baier, M. Fontannaz and D. Schiff, Nucl. Phys. **B297** (1988) 661.
- [34] P.M. Stevenson, Phys. Rev. **D23** (1981); H.D. Politzer, Nucl. Phys. **B194** (1982) 493; P.M. Stevenson and H.D. Politzer, *ibid.* **277**, 758 (1986).
- [35] L.E. Gordon and W. Vogelsang, Phys. Rev. **D48** (1993) 3136.
- [36] M. Glück, E. Reya and A. Vogt, Z. Phys. **C48** (1990) 471.

- [37] P. Aurenche, R. Baier and M. Fontannaz, Phys. Rev. **D42** (1990) 1440.
- [38] S. Kuhlmann, *private communication*.
- [39] M. Stratmann and W. Vogelsang, Univ. Dortmund report DO-TH 94/23, to appear in Phys. Rev. **D**.
- [40] M. Glück, E. Reya and A. Vogt, Phys. Rev. **D45** (1992) 3986, **D46** (1993) 1973.
- [41] E.W.N. Glover and A.G. Morgan, Z. Phys. **C62** (1994) 311; J.C. Thompson, ALEPH Collab., *private communication*.
- [42] A. Vogt, DESY 95-068, to appear in Phys. Lett. **B**.
- [43] A. Milsztain and M. Virchaux, Phys. Lett. **B274** (1992) 221.
- [44] M. Arneodo et al., NMC Collab., Phys. Lett. **B309** (1993) 222.
- [45] P.Z. Quintas et al., CCFR Collab., Phys. Rev. Lett. **71** (1993) 1307.
- [46] W.J. Stirling, *private communication*.
- [47] G. Alverson et al., E706 Collab., Phys. Rev. Lett. **68** (1992) 2584; Phys. Rev. **D48** (1993) 5; *ibid.* **D49** (1994) 3106.
- [48] F. Abe et al., CDF Collab., Phys. Rev. Lett. **71** (1993) 500, 2396.
- [49] S. Abachi et al., D0 Collab., Phys. Rev. Lett. **74** (1995) 3548.
- [50] P. Nason, S. Dawson and R.K. Ellis, Nucl. Phys. **B303** (1988) 607.
- [51] E. Laenen, S. Riemersma, J. Smith and W.L. van Neerven, Nucl. Phys. **B392** (1993) 162.

## Figure Captions

**Fig. 1:** The ‘default quantity’  $(\sigma_{exp} - \sigma_{th})/\sigma_{th}$  vs.  $x_T = 2p_T/\sqrt{s}$  for the data of [1, 14, 15, 18] as compared to the NLO theoretical cross section  $\sigma_{th}$ , using the GRV parton distributions and photon fragmentation functions [4, 26]. The curves present the shifts  $(\sigma_{th'} - \sigma_{th})/\sigma_{th}$ , where  $\sigma_{th'}$  denotes the theoretical cross section if the fragmentation contribution is neglected or if the fragmentation functions of [25] are used.

**Fig. 2:** Comparison of the fragmentation functions  $zD_u^\gamma(z, Q^2)/\alpha$  and  $zD_g^\gamma(z, Q^2)/\alpha$  from ACFGP [25] and GRV [26] at  $Q^2 = 10$  and  $100 \text{ GeV}^2$ .

**Fig. 3:** NLO  $\overline{\text{MS}}$  fragmentation piece for the ACFGP [25] and GRV [26] photon fragmentation functions at ISR and Tevatron energies, using the CDF isolation criterion in the latter case. Also shown are the contributions stemming from gluon-to-photon fragmentation only. All cross sections are normalized to the NLO direct piece. The parton distributions of [4] are used and the scales are  $\mu_R = \mu_F = 0.5 p_T$ .

**Fig. 4:** Same as Fig. 1, but the lines displaying the shifts in the theoretical results if the renormalization and factorization scales are varied as indicated in the figure.

**Fig. 5:** The data of [1, 14, 15, 18] as compared to three NLO fits for the different choices of  $\Lambda_{\overline{\text{MS}}}$  and of the scales indicated in the figure. The CDF data [18] are shown with their fitted normalizations.

**Fig. 6:** Comparison of the gluon distributions obtained in the three fits displayed in Fig. 5 with the MRS(A') [2] gluon density.  $\bar{\Lambda}$  denotes  $\Lambda_{\overline{\text{MS}}}^{(4)}$  in MeV.

**Fig. 7:** The cross section for single-inclusive bottom production,  $\sigma(p\bar{p} \rightarrow bX)$ , as a function of the minimal transverse momentum  $p_T^{\text{min}}$  of the  $b$ -quark as calculated in NLO perturbative QCD using the parton distributions indicated in the figure. Also shown are the (inclusive lepton) data of [48, 49].

**Fig. 8:** The error bands of the fitted gluon densities due to scale variations for the fit to all data and for the fit retaining the (non-isolated) fixed-target [1, 8, 16] and ISR [14] prompt photon data only, plotted via the deviation from the MRS(A') fit. Also displayed are the  $1\sigma$  uncertainties resulting from the experimental errors and two further 'standard' gluon parametrizations [2, 4].

**Fig. 9:** Same as Fig. 8, but for the absolute gluon distributions at large  $x$  at a typical scale probed by the direct- $\gamma$  data (left) and at a very large scale relevant for the production of very heavy particles (right). Of the rather similar 'standard' gluons only the one of MRS(A') [2] is shown for comparison.

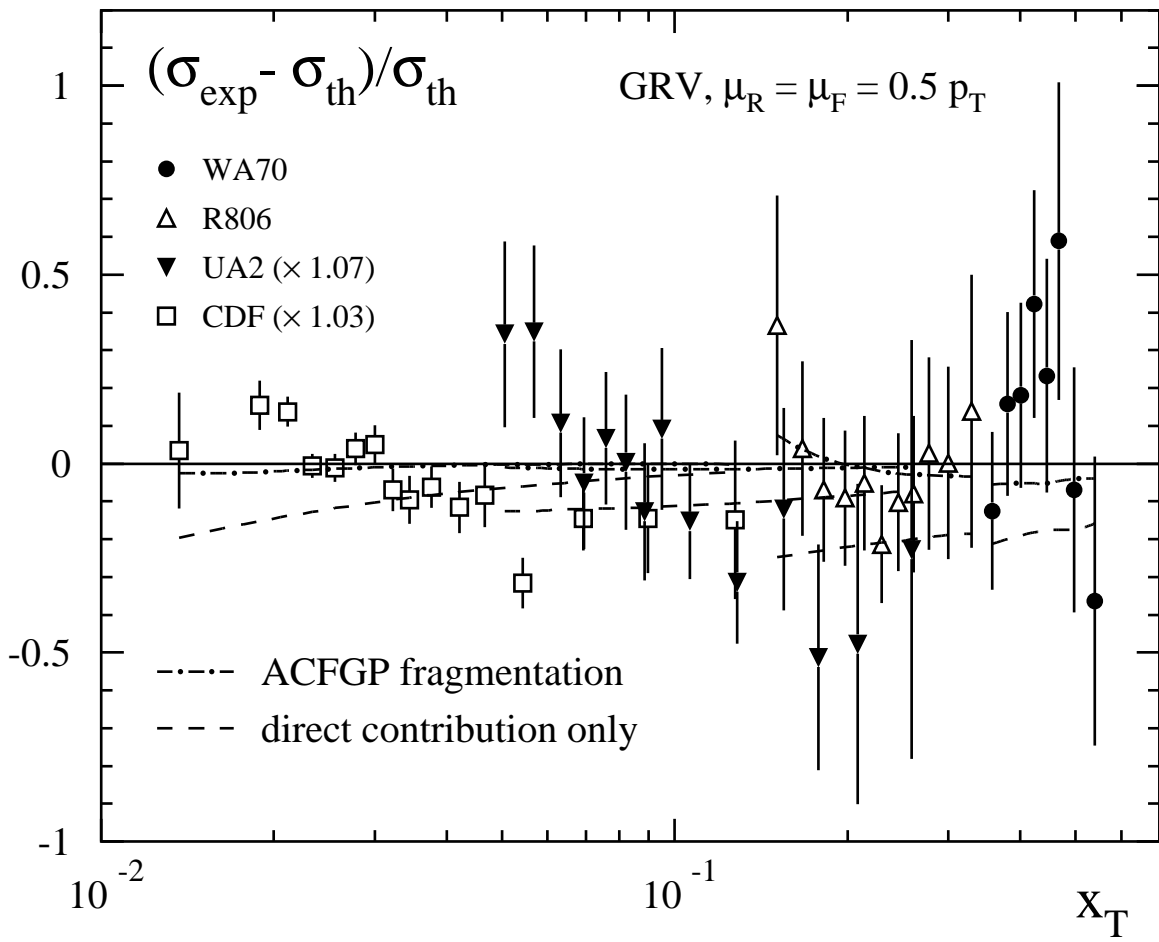


Fig. 1

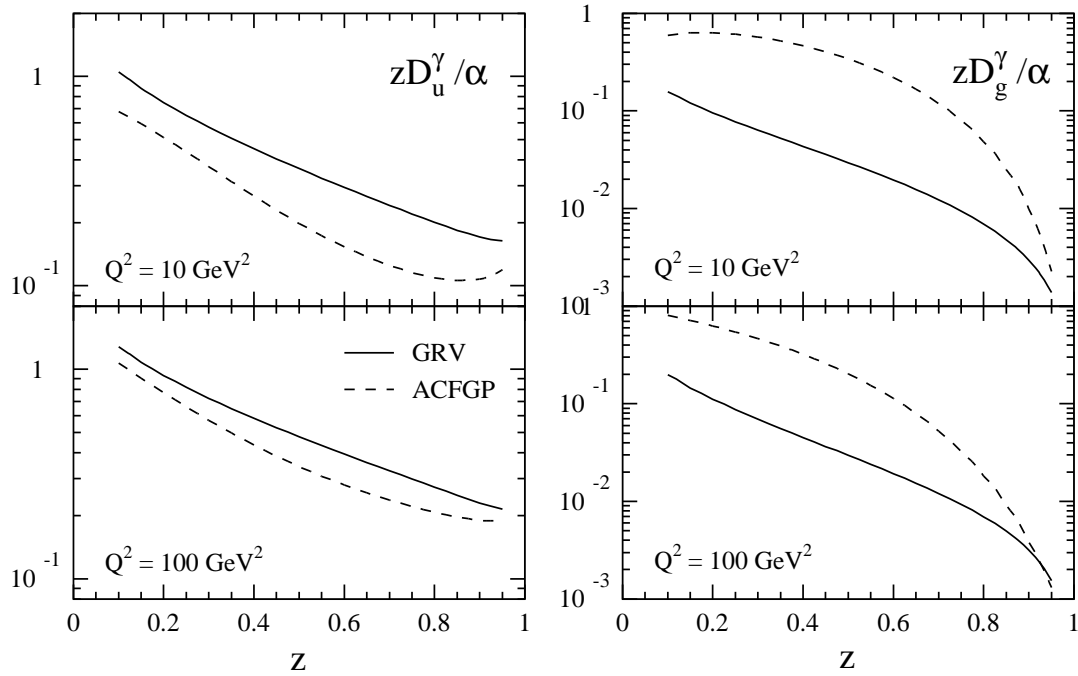


Fig. 2

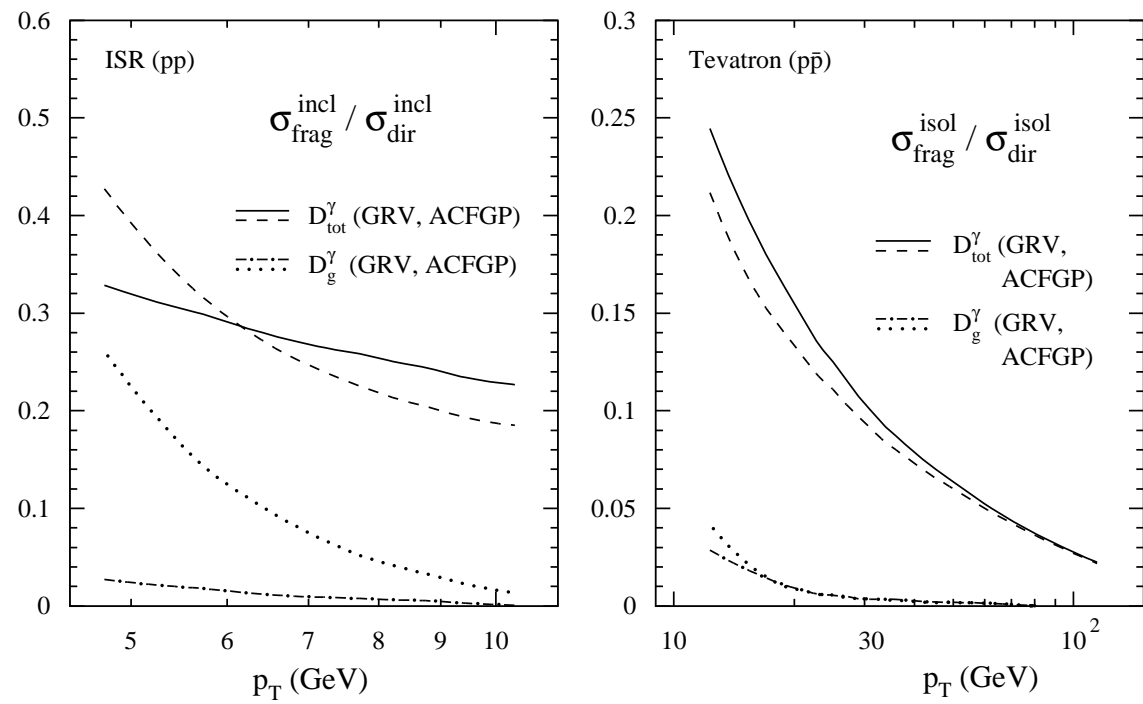


Fig. 3

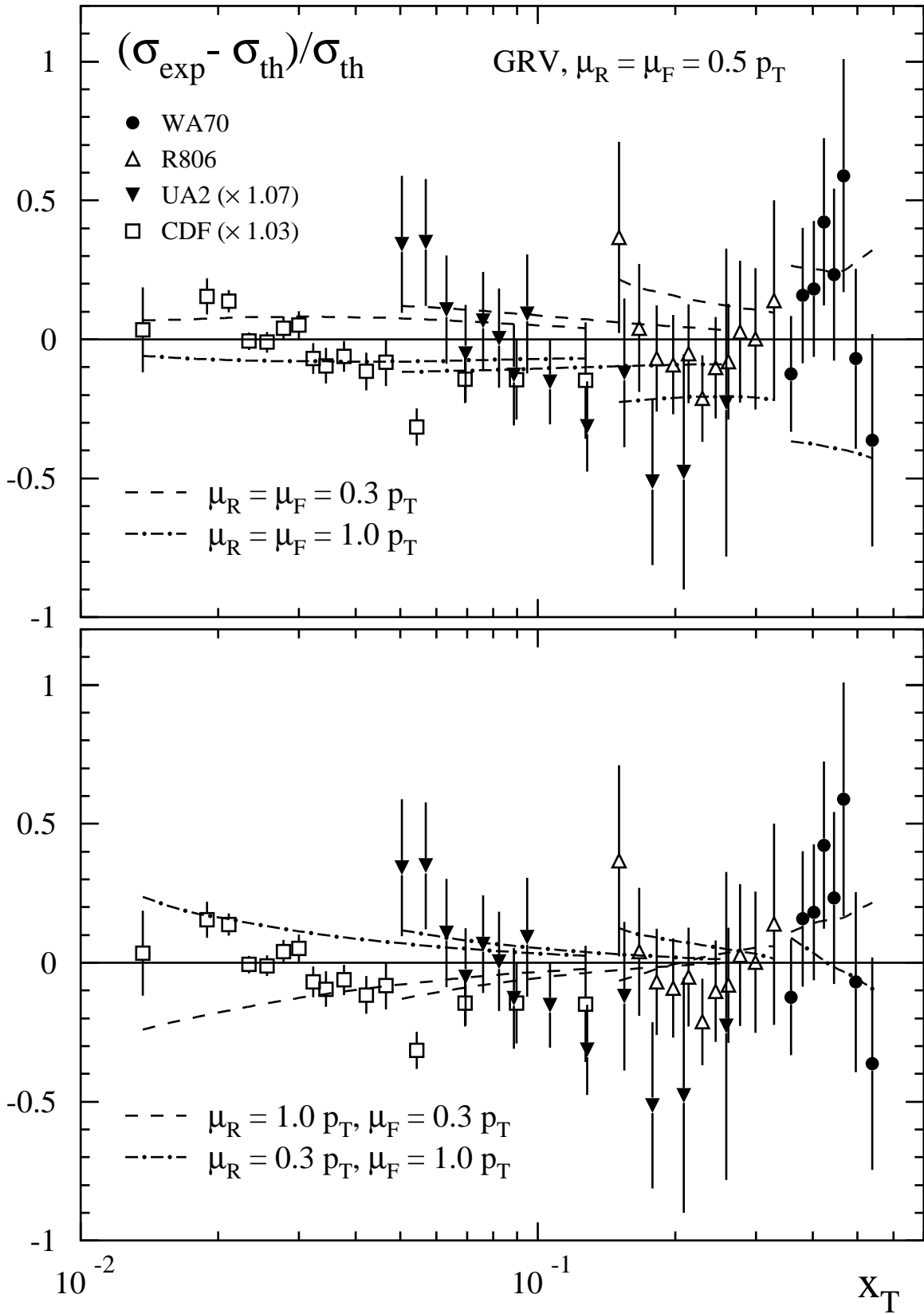


Fig. 4



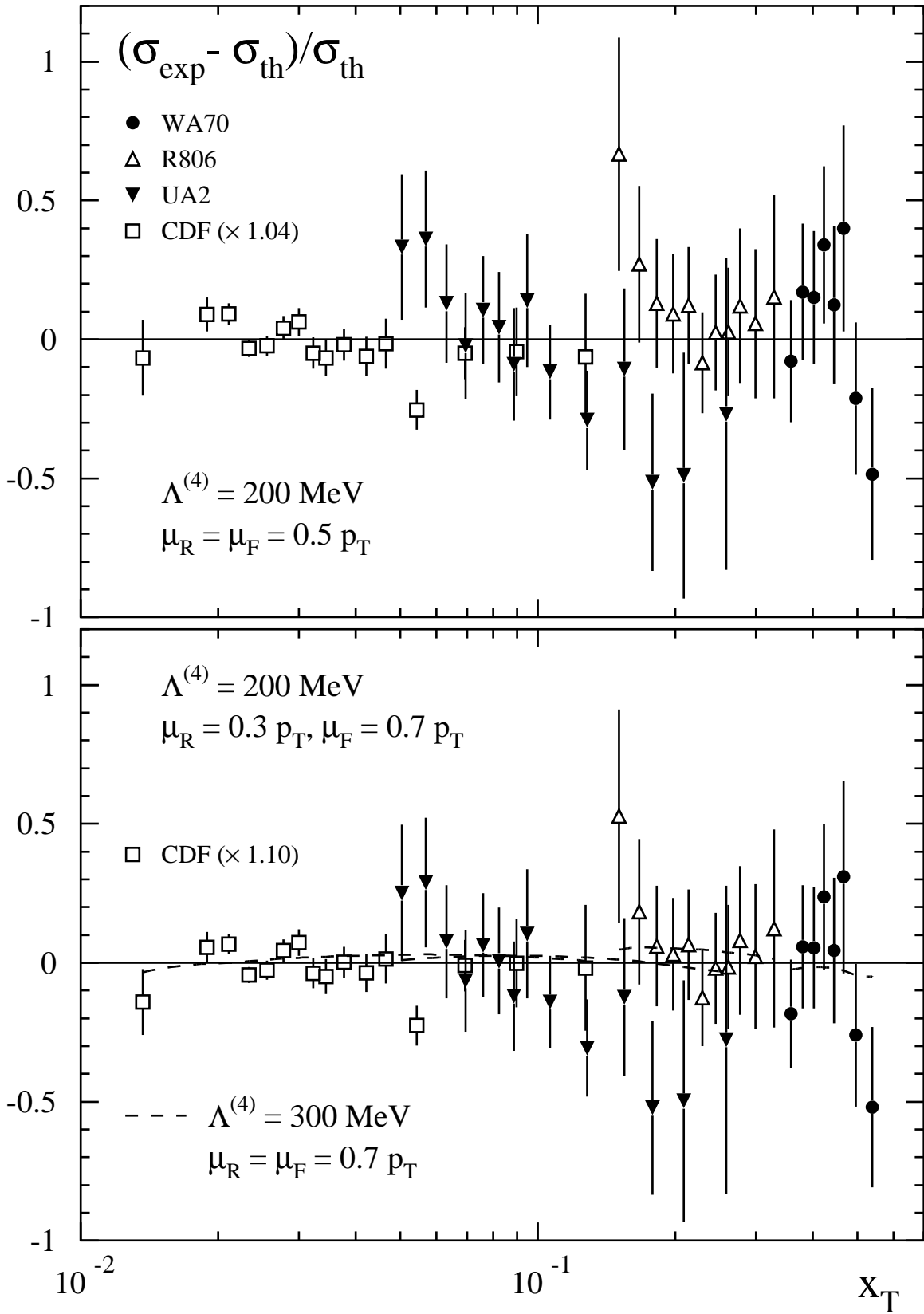


Fig. 5

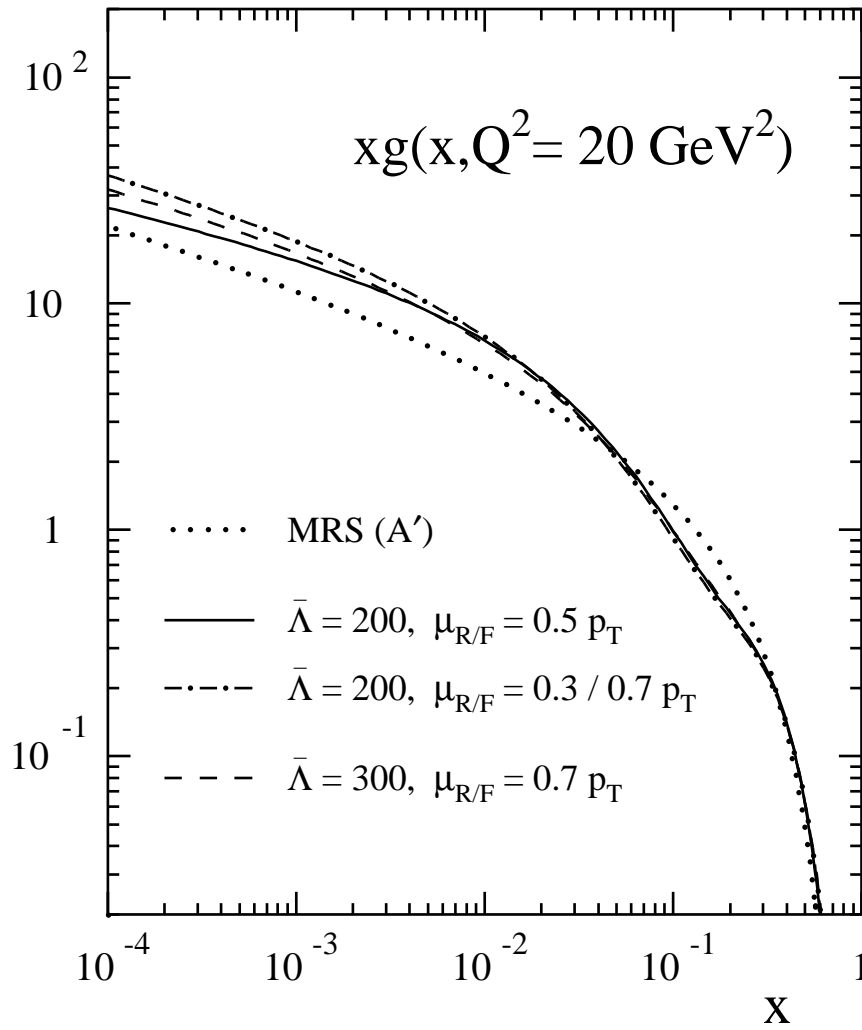


Fig. 6

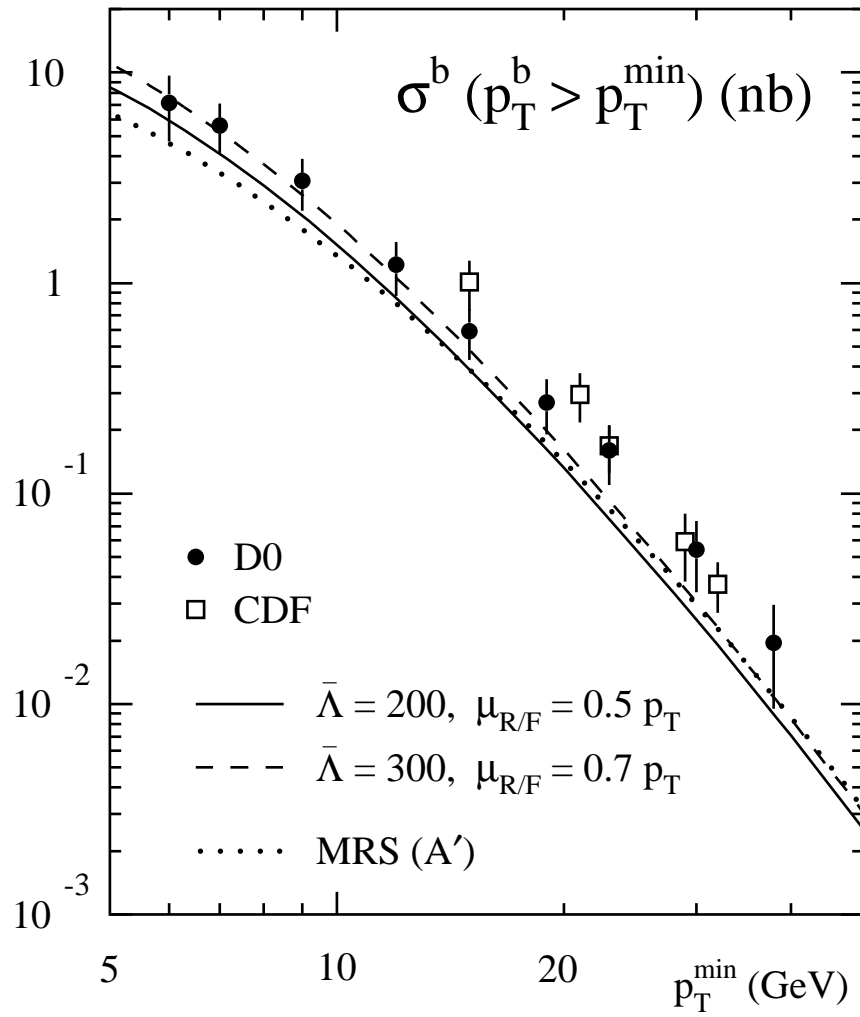


Fig. 7

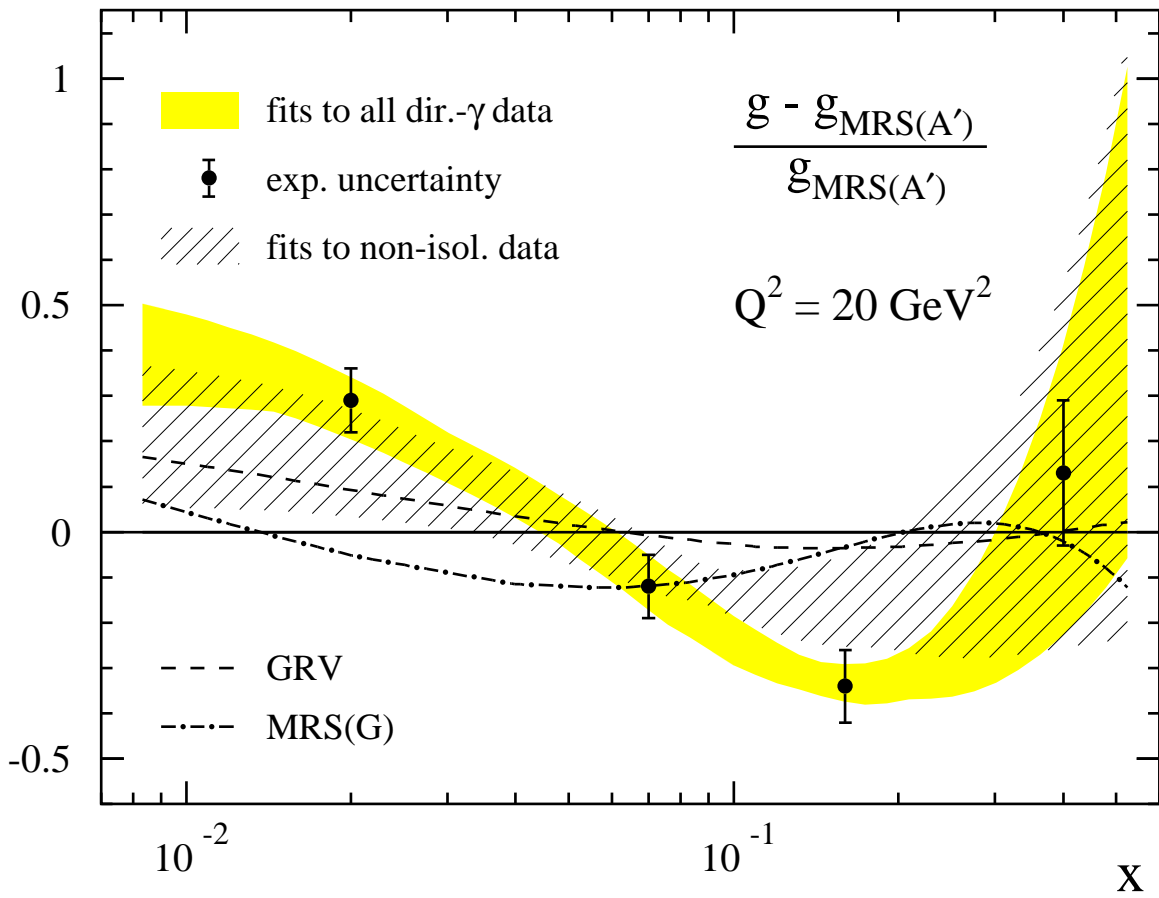


Fig. 8

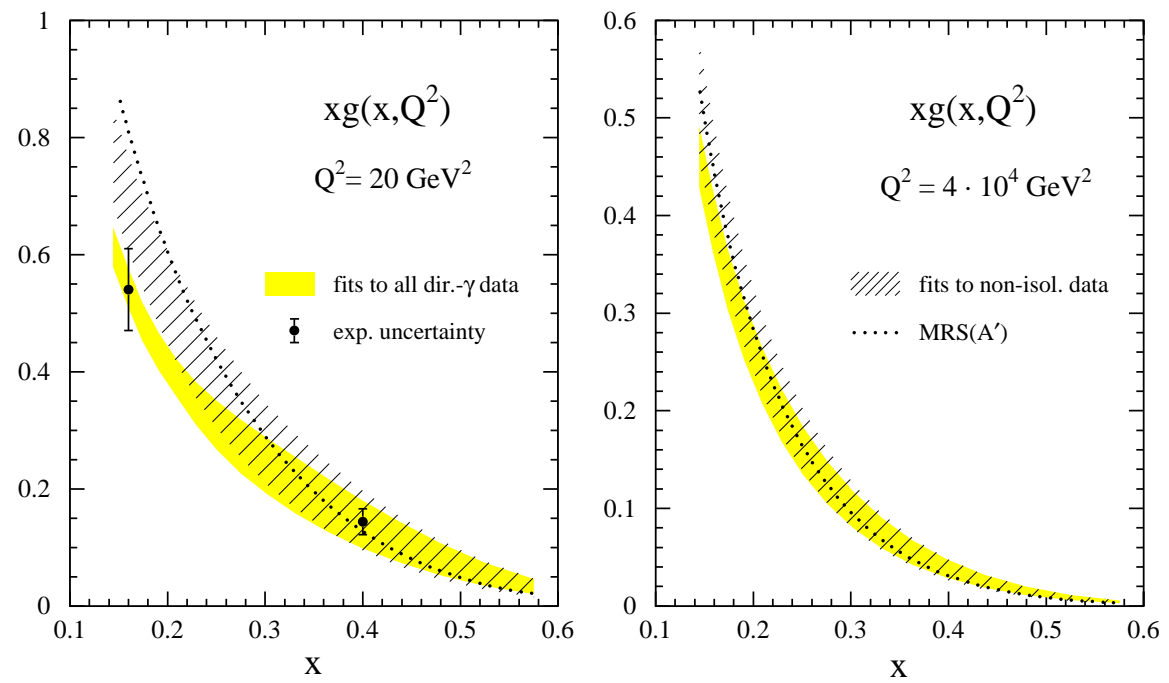


Fig. 9